Chapter 7. Granite Geochemistry

7.1 Introduction

Field relationship, microstructures and geochemical signatures of granites are used as tools to decipher nature of plutonic emplacement and associated tectonic environment. As field relationships of these granites and microstructures, have already been discussed in chapters 3 and 5, respectively, the present chapter mainly focuses on the geochemical signatures in terms of concentration, variation and distribution of the major oxides, trace and REE elements, of granites exposed in the vicinity of Champaner Group. The samples obtained from the study area were processed to analyze major oxides through X-ray Fluorescence (XRF) spectrometer and trace elements by Inductively Coupled Plasma Mass Spectrometry (ICP-MS).

7.2 Methodology

The methodology followed right from sample collection to the sample preparation for geochemical analyses. The fresh and adequate amount of 40 samples was procured from the field. Among them, best 10 representative samples were selected region wise for geochemical analyses, viz. TMG-1; TMG-2;…; TMG-10. These samples were powdered in the tungsten-carbide ball mill and processed further for geochemical analyses using XRF and ICP-MS at Physical Research Laboratory (PRL) Ahmedabad.

7.2.1 Sample Preparation for XRF-analysis

In order to prepare sample for XRF studies, the acquired powder was homogeneously mixed in an agate mortar with the wax binder having proportion of 4:1. The homogenised mixture was filled into standard aluminium cups in order to impart high pressure of 160 kN for approximately 3 minutes. The pressure was withdrawn slowly and pellets were acquired. These pellets were used for major oxides analyses.

7.2.2 Sample Preparation for ICP-MS analysis

In order to prepare samples for ICP-MS analysis, the powdered samples were dissolved through following specific chemical and physical treatments:

- 50 mg of samples was taken in the special vials to avoid the contamination.
- 1.5 ml 8N HNO_3 (nitric acid) and 0.5 ml HF (hydrofluoric acid) was added into the vials.
- These vials were tightly closed and placed into the framework of Microwave Digestion System. (Note: Microwave Digestion System is a special setup, which heat the samples at particular pressure and temperature path to produce completely dissolved samples within relatively shorter time period).
- The dissolved sample was further diluted through 8N HNO_3 to make 50 ml sample in total.

7.2.3 Method to calculate Loss-On-Ignition (LOI)

The powdered samples were first weighed on weighing scale. The weighed samples were kept in furnace having temperature more than 1000^{o}C for about 1 hour. Once the samples attained room temperature they were reweighed to calculate the weight loss. Percentage of the weight loss has been considered as LOI. The geochemical data has been normalized by using the LOI.

7.3 Modal Analyses

Granites of the study area are medium to coarse grained and contain quartz, feldspars, biotite and hornblende as essential minerals, whereas apatite, zircon, epidote and opaques as accessory minerals. Results from the above analyses (Table. 7.1), suggest that these granites contain plagioclase as a dominant mineral (43.04-27 vol. %) with K-feldspar (33-15.9 vol. %), quartz (32-20.5 vol. %) and biotite (13-6.7 vol. %), except for two samples where presence of hornblende ranges between (5.8-2.8 vol. %). Other minerals such as opaques, muscovite, zircon, apatite and epidote are in minor amounts. The plot of modal composition in QAP (quartz, alkali-feldspar and plagioclase) triangular diagram (Streckeisen, 1974), suggests that the granites of the study area falls in monzogranite to granodiorite in composition (Fig. 7.1) viz. the samples collected from north of Singpur (TMG01) and south-east of Valothi (TMG03) fall in granodiorite field, whereas rest are of monzo-granite variety.

Sample Number	TMG 01	TMG 02	TMG 03	TMG 04	TMG 05	TMG 06	TMG 07	TMG 08	TMG 09	TMG 10
Quartz	23	28.7	20.8	22.5	27	20.5	25	22	26	32
Plagioclase	41	34.3	43.04	34	33.4	27	36	35	31	28
K-feldspar	21.6	21.2	15.9	27.9	28	33	24.6	27	22	23
Biotite	6.7	9.3	13	9.7	6.8	12	10	11	13	9
Muscovite	2.1	0.2	Nil	0.5	1	2	1	0.4	0.1	2
Hornblende	Nil	Nil	5.8	Nil	Nil	Nil	Nil	Nil	2.8	1.3
Opaques	5.1	4.4	3	3.8	3.3	5	4.5	6	4	4
Others	0.5	0.3	0.2	0.3	0.4	0.2	0.1	0.3	0.4	0.3

Locations of granite samples: TMG01= N of Singpur; 02= NNW of Hirapur; 03= SE of Valothi; 04= E of Shivjipura; 05= S of Dhanpur (Makhaniya dungar, near Sukhi dam); 06= W of Lambhiya; 07= Kanpur; 08= Ranjitnagar; 09= S of Bhulvan; 10= NE of Bodeli.

Table: 7.1: Modal compositions of various granite samples in and around Champaner Group.

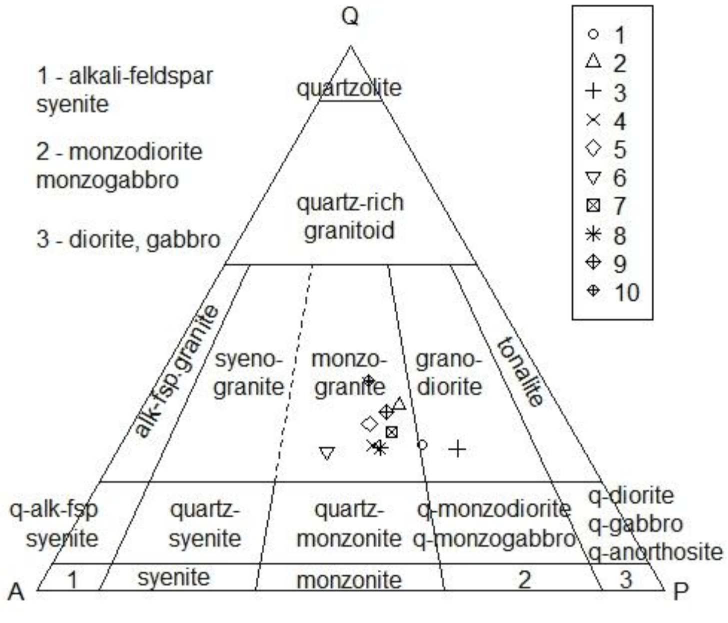

Figure 7.1: QAP diagram, after Streckeisen, 1974.

7.4 Major and Trace element geochemistry

Geochemically, the granites of study area show variable concentration of major oxides (Table. 7.2a). The SiO_2 and Al2O3 ranges from 62.2 wt% to 69.9 wt% and 15.4 wt% to 17.2 wt%, respectively. Other than SiO_2 and Al_2O_3, the K_2O and Fe_2O_3 oxides are present in noticeable amounts, K_2O concentration vary between 4.17 wt% and 6.53 wt% and Fe_2O_3 between 3.19 wt% and 5.94 wt%. The Na_2O and CaO contents show variation between 2.45 wt% to 3.65 wt% and 0.55 wt% to 3.64 wt%, respectively. The MgO content within these granites ranges from 1.93 wt% to 3.54 wt%. Most of the Fe-Mg content is in biotite, as it is a major ferromagnesian mineral present within the granites of the study area. Oxides such as P_2O_5, MnO and TiO_2 are present in minor amounts. Based on the major oxides data, Harker bivariate plot has been generated through Geo-Chemical Data kit (GCDKit) software (Fig. 7.2). The plots suggest the degree of fractionation and trend in which the granitic magma has been evolved.

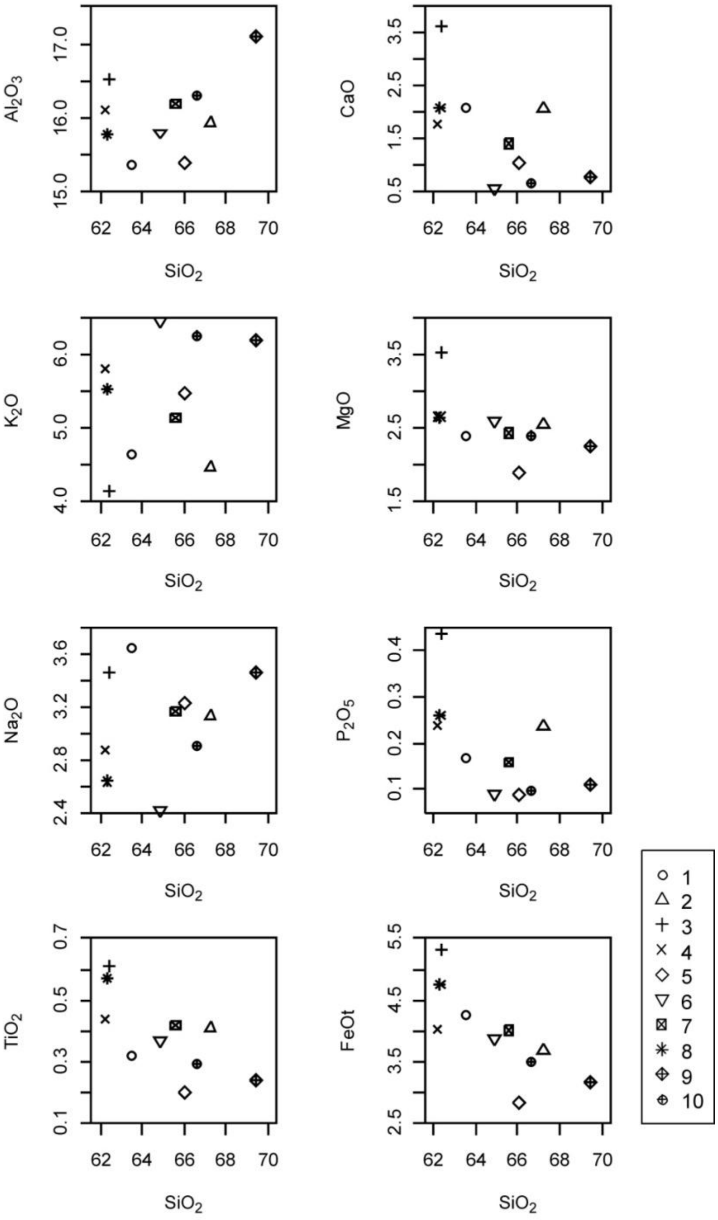

Figure. 7.2: Harker Bivariate plots

(a) Major oxides in Wt%	**TMG1**	**TMG2**	**TMG3**	**TMG4**	**TMG5**	**TMG6**	**TMG7**	**TMG8**	**TMG9**	**TMG10**
SiO_2	63.7	67.5	62.7	62.2	66.9	65.7	66	62.4	69.9	67.8
TiO_2	0.32	0.41	0.61	0.44	0.2	0.37	0.42	0.57	0.24	0.3
Al_2O_3	15.4	16	16.6	16.1	15.6	16	16.3	15.8	17.2	16.6
Fe_2O_3(T)	4.74	4.12	5.94	4.46	3.19	4.34	4.48	5.3	3.54	3.94
MnO	0.07	0.06	0.08	0.07	0.06	0.05	0.06	0.07	0.06	0.05
MgO	2.39	2.56	3.54	2.66	1.93	2.62	2.45	2.66	2.28	2.45
CaO	2.08	2.07	3.64	1.78	1.05	0.55	1.42	2.1	0.78	0.66
Na_2O	3.65	3.14	3.48	2.87	3.27	2.45	3.19	2.64	3.48	2.96
K_2O	4.67	4.48	4.17	5.8	5.55	6.53	5.17	5.54	6.22	6.37
P_2O_5	0.17	0.24	0.44	0.24	0.09	0.09	0.16	0.26	0.11	0.1
LOI %	0.267	0.388	0.5	0.56	1.29	1.23	0.63	0.12	0.668	1.76
Total	97.457	100.968	101.7	97.18	99.13	99.93	100.28	97.46	104.478	102.99
A/CNK	1.48	1.65	1.47	1.54	1.58	1.68	1.67	1.54	1.64	1.66

(b) Trace Elements in ppm	**TMG1**	**TMG2**	**TMG3**	**TMG4**	**TMG5**	**TMG6**	**TMG7**	**TMG8**	**TMG9**	**TMG10**
Sc	49.6	17.2	38.1	29.1	43.8	65.7	79.6	70.7	76.6	38.4
V	31.3	26.5	61.8	27.5	4.46	0	20.9	89.4	3.25	6.48
Cr	163	118	122	88.8	141	127	147	195	140	236
Co	3.18	3.63	9.16	5.92	1.31	1.41	4.43	14.1	1.18	1.02
Ni	-	-	5.09	-	-	-	6.24	5.22	-	-
Sr	398	269	553	239	99	12.4	128	291	65.6	192
Y	17.9	12.4	27.3	15	2.97	6.36	5.91	31.8	3.16	7.7
Zr	347	244	228	210	226	230	175	353	142	206
Nb	30.3	16.1	21.6	14.2	25.2	29.3	16.8	22.5	14.8	29.2
Ba	509	873	1473	1114	561	470	598	1585	607	917
Cs	1.78	2.08	3.37	2.84	7.56	1.51	5.87	7.12	1.64	4.04
Rb	114	59	68.2	94.5	226	105	125	127	113	156
La	25.3	26.4	53.7	37.2	4.28	2.36	6.7	16.5	2.88	5.94
Ce	55.7	69.9	129	93.9	13.9	8.15	18.3	44.1	12.3	23.5
Pr	5.92	7.3	14.4	10.1	1.27	0.98	2.01	5.17	0.88	2
Nd	20.3	25.8	51.6	35	4.76	4.08	7.06	19.2	3.09	7.74
Sm	3.9	4.6	9.3	6.4	1.05	1.42	1.64	4.24	0.84	1.8
Eu	0.77	1.07	1.94	1.23	0.24	0.33	0.49	1.21	0.21	0.41
Gd	3.26	3.56	7.4	5.09	0.69	1.12	1.17	3.75	0.43	1.35
Tb	0.5	0.51	1.04	0.73	0.14	0.29	0.22	0.69	0.11	0.26
Dy	2.8	2.71	5.25	3.45	0.93	2.12	1.43	4.21	0.79	1.74
Ho	0.57	0.53	1.03	0.66	0.17	0.42	0.28	0.88	0.18	0.32
Er	1.78	1.52	2.92	1.78	0.53	1.35	0.82	2.6	0.58	0.98
Tm	0.26	0.21	0.38	0.23	0.07	0.2	0.11	0.34	0.09	0.14
Yb	1.96	1.48	2.62	1.61	0.55	1.5	0.83	2.49	0.72	1.13
Lu	0.33	0.23	0.37	0.23	0.08	0.22	0.12	0.37	0.11	0.16
Hf	8.9	6.86	6.04	6.09	6.22	6.74	4.96	6.47	4.41	5.38
Ta	2.39	1.22	1.72	1	3.42	2.32	1.85	1.51	1.78	2.36
Pb	15.4	25.6	23.4	29.9	32	6.99	25	28.7	16	47.1
Th	28.3	17.1	11	27.6	14.1	9.44	11.4	19.9	15.1	24.3
U	12.9	3.87	5.14	2.67	4.45	3.82	3.55	3.89	6.18	7.68

Table 7.2: (a) Major oxides and (b) Trace element concentration in granites.

Harker bi-variate plots suggest that the granites of the study area show negative correlation of P_2O_5, TiO_2, Fe_2O_3(T), MgO and CaO with SiO_2 concentration. The concentration of Na_2O show independent relationship with respect to that of SiO_2. In case of Al_2O_3 and K_2O concentration, a weak positive correlation has been observed. These positive and negative correlations within the major oxides depict the effect of fractional crystallisation during emplacement of granitic pluton. The negative correlations of P_2O_5, TiO_2, FeO(T), MgO and CaO oxides with respect to SiO_2 concentration suggest that there has been an accommodation of these elements present within these oxides into mineral phases that crystallised during the early period of magma cooling such as apatite and ilmenite leading to fractionation of the magma. Similarly, the positive correlation between Al_2O_3, K_2O and SiO_2 are consistent with crystallization and accumulation of feldspar and hence indicate an enrichment of Al, K and Si.

Trace elements concentration within the granites of the study area shows enrichment of LREE (light rare earth elements) over HREE (heavy rare earth elements) (Table. 7.2b). The present enrichment can be easily appreciated through the fractionated chondrite normalized REE pattern (Fig. 7.3).

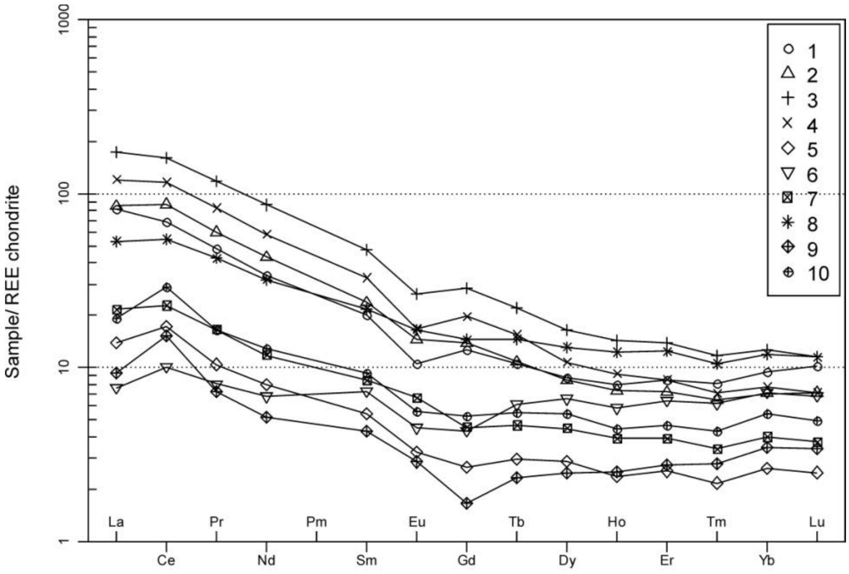

Figure 7.3: REE Chondrite normalized plot (Boynton 1984) suggesting higher LREE content over HREE.

The clear trend of enriched LREE over HREE is observed with faint Eu-anomaly. These LREE enrichment and Eu-anomaly suggests either earlier fractionation of plagioclase or the presence of plagioclase in the source region. Two probable explanations can be given for the depleted HREE concentrations: 1. The depletion of HREE is predominantly caused by low degree of melting of garnet-rich sources which retains and depletes the melt in HREE (Drummond and Defant, 1990; Martin et al., 2005). 2. The late stage fractionation of heavy mineral phases like zircon, allanite, sphene, apatite and monazite is because of their extremely high partition coefficient for HREE (Gromet and Silver, 1983; Rollinson, 1993). Some important trace elements has concentration (in ppm) as follows, Sc-17.2 to 76.6, V-3.25 to 89.4, Cr- 88.8 to 236, Co- 1.02 to 4.43, Sr- 65.5 to 553, Y- 2.97 to 31.8, Zr- 142 to 353, Ba- 470 to 1585, Rb- 59 to 226, Eu- 0.21 to 1.94, Pb- 6.99 to 47.1, Th- 9.44 to 28.3, U- 2.67 to 12.9. The Harker binary plots (Fig. 7.4) signify that the Sr, Y, Zr and Cr demarcate negative correlation with SiO_2 suggesting that these elements have been accommodated within the mineral phases which were crystallized earlier in the magma. A weak positive correlation of Rb suggests that the accommodation has lasted till late phase of crystallisation. Barium concentration of granites plotted against SiO_2 suggests non-linear relationship; however the distinct positive correlation of Ba with Sr suggests a systematic removal of biotite and plagioclase from the melt.

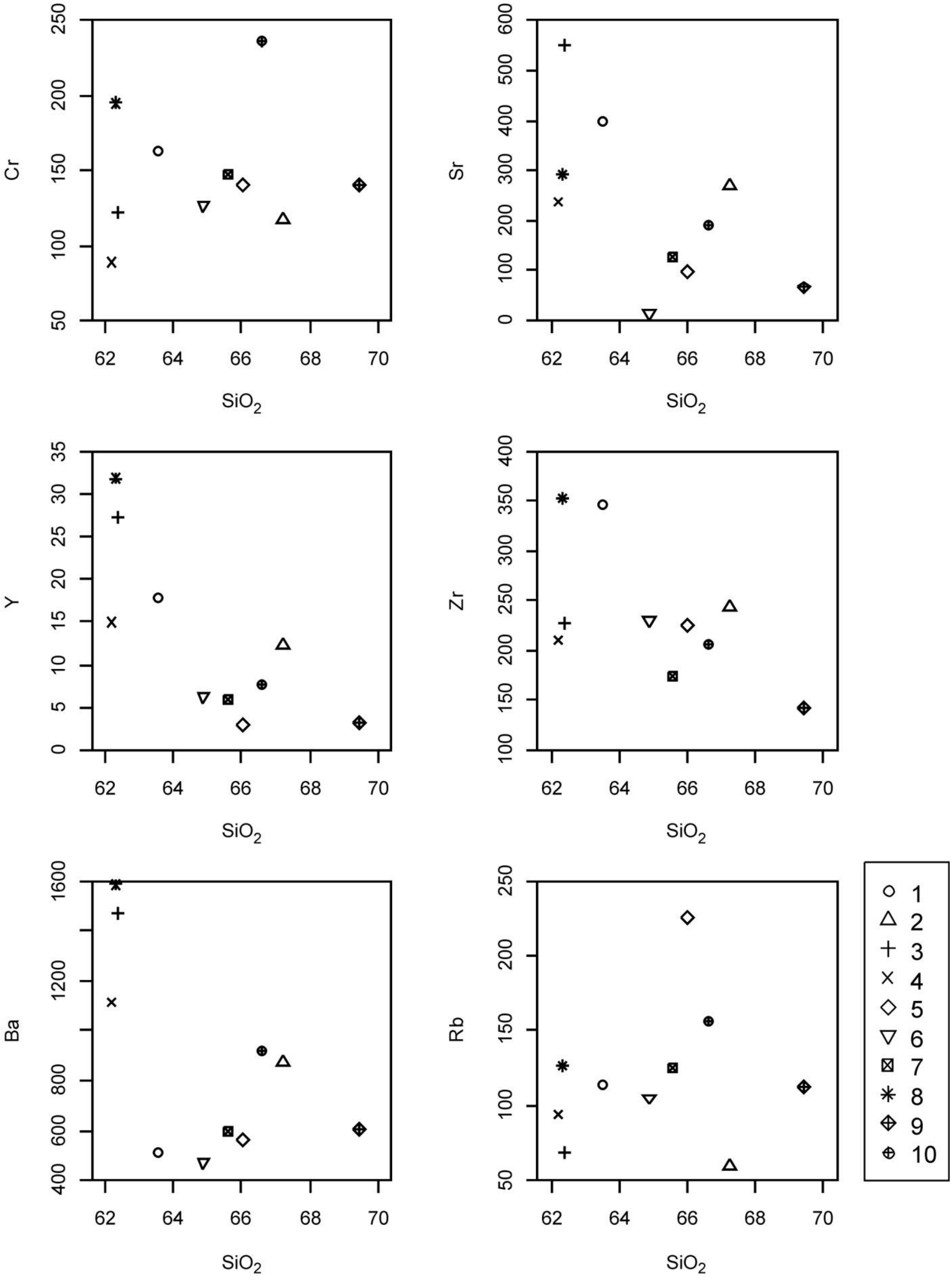

Figure: 7.4: Harker bi-variate plots of SiO_2 vs trace elements. The Cr,Sr,Y and Zr shows moderate negative correlation with SiO_2 whereas, Ba and Rb do not show any distinct trend.

7.5 Tectonic Implications

In order to establish the tectonic environment of the granites associated in and around Champaner Group, Maniar and Piccoli, (1989) has used various major oxides and their ratios such as M/AFM vs F/AFM, C/ACF vs F/ACF, etc. to broadly discriminate the granites. They have discriminated granites into seven types, on the basis of SiO_2 vs K_2O plots, viz. oceanic-plagiogranites (OP) to island arc granitoids (IAG), continental arc granitoids (CAG), continental collision granitoids (CCG), rift related granitoids (RRG), continental epiorogenic uplift granitoids (CEUG) and postorogenic granitoids (POG). M/AFM vs F/AFM plot discriminate the granites from RRG and CEUG and suggest the possible IAG, CAG or CCG type, however the samples of the study area shows affinity towards field of POG. C/ACF vs F/ACF plot shows distribution of samples in and near the field of POG, whereas few samples fall in IAG+CAG+CCG field. Lastly, the distribution of samples in peraluminous field of A/CNK vs A/NK plot suggests affinity towards continental collision granites (CCG) or post orogenic granites (POG) (Fig. 7.5). Another plot using major oxide data, suggested by Batchelor and Bowden, (1985) (R1-R2 plot) clearly indicate that the granites of study area as syn-collision granites. Within the syn-collision granite’s field of R1-R2 plot the samples are plotted in sub-fields of late orogenic type and post-collision uplift type granites. However, majority of samples point to late orogenic subfield of syn-collision granites (Fig. 7.6).

Various tectonic discrimination diagrams suggested by Pearce et al., (1984) using trace element data have also been plotted for the granites of the study area. The results are in accordance with the earlier discrimination diagrams. According to Pearce et al., (1984), the Y versus Nb plot differentiates these granites from the category of within plate granites (WPG) and oceanic ridge granites (ORG). The Y+Nb and Ta+Yb versus Rb diagrams suggest the post-collisional environment of emplacement with affinity of samples tending more towards the syn-collisional field. The Yb versus Ta plot discriminate the granites from volcanic arc granites (VAG) and suggests those of syn-collision type (Fig. 7.7).

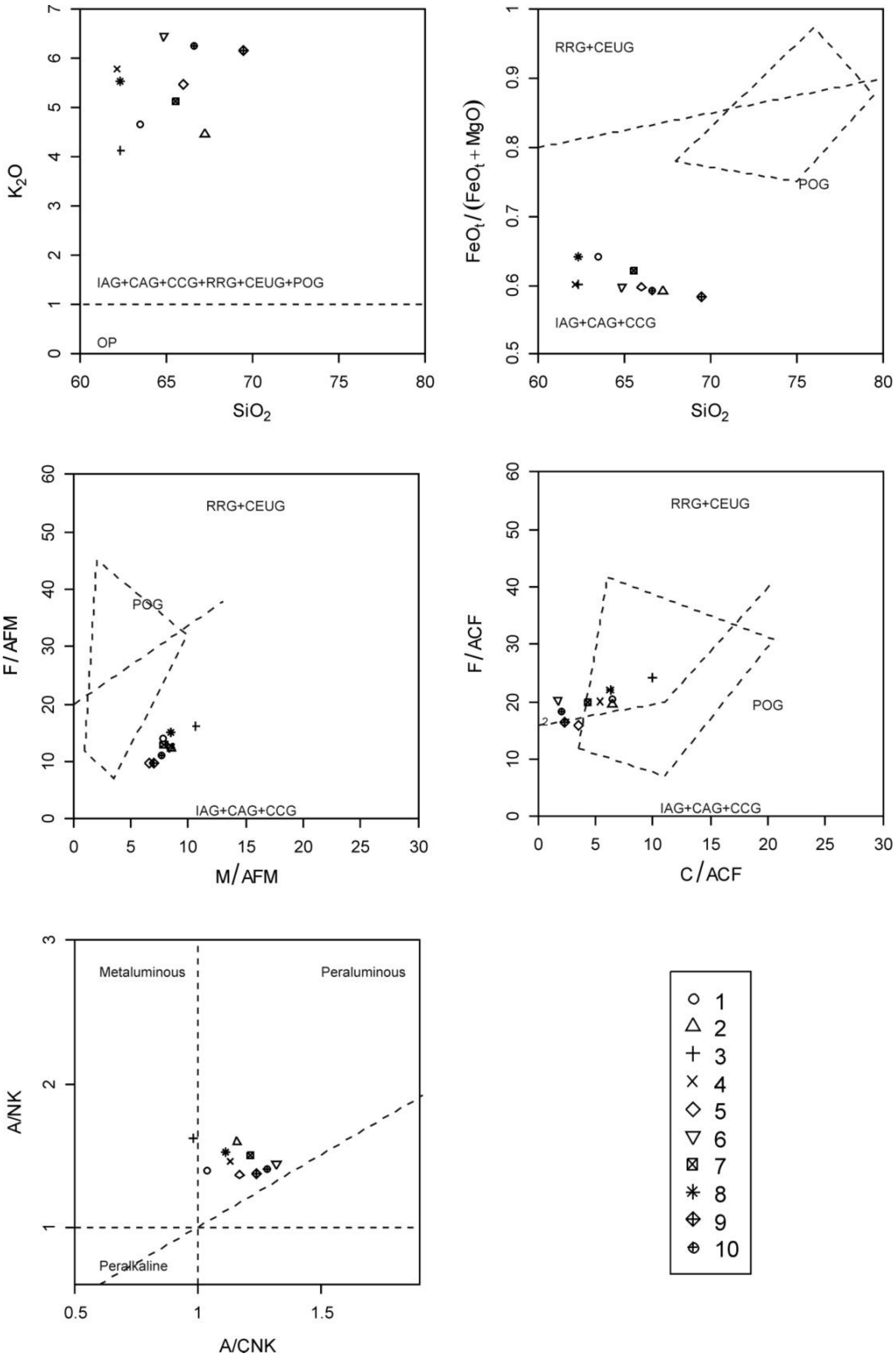

Figure. 7.5: The tectonic discriminatory plot by Maniar and Piccoli (1989). IAG= Island Arc Granitoids, CAG= Continental Arc Granitoids, CCG = Continental Collision Granitoids, POG = Postorogenic Granitoids, RRG = Rift related Granitoids, CEUG = Continental epiorogenic uplift Granitoids, OP = Oceanic Plagiogranites.

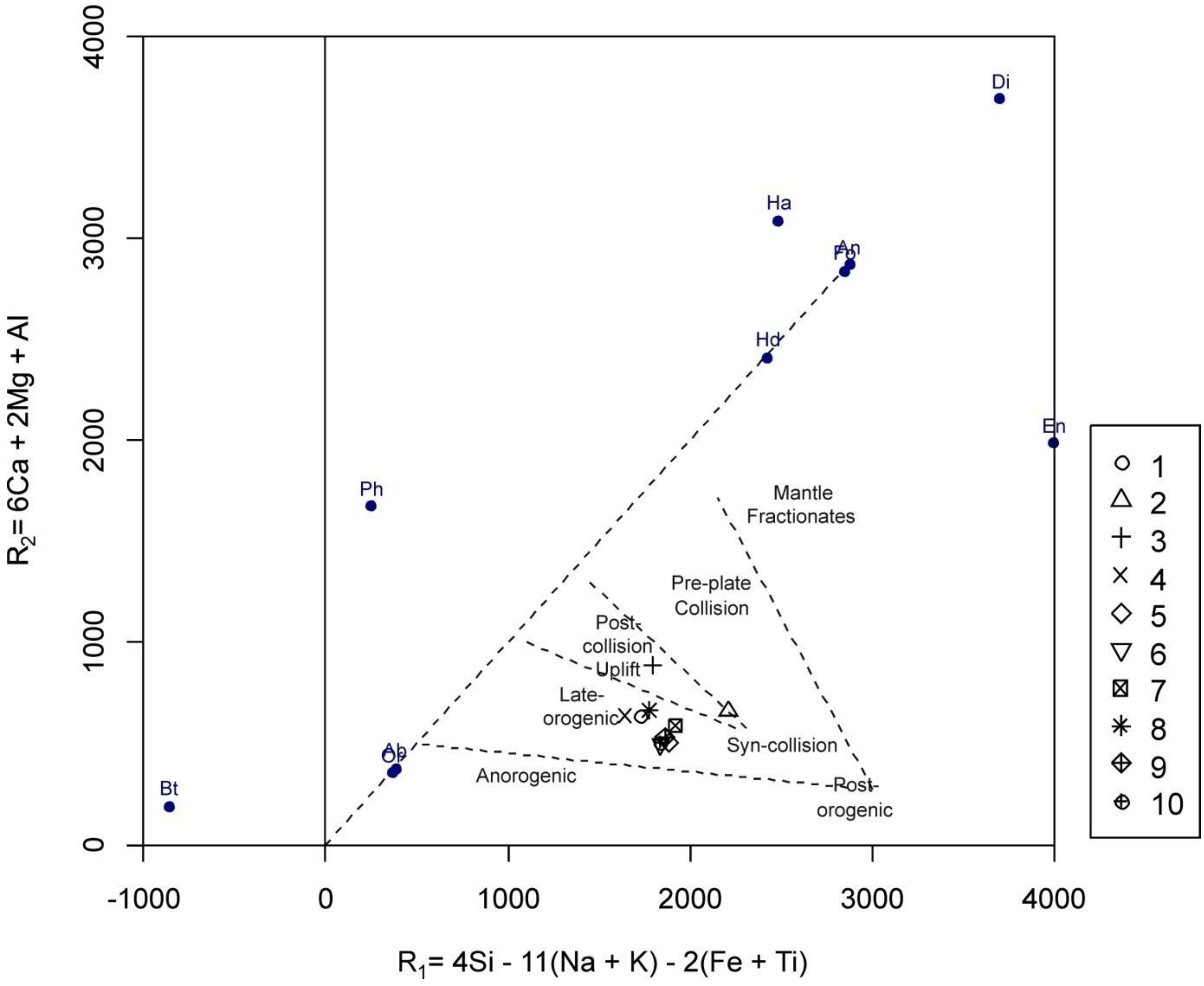

Figure. 7.6: R1-R2 plot by Batchelor and Bowden, (1985) for tectonic discrimination of granites of study area.

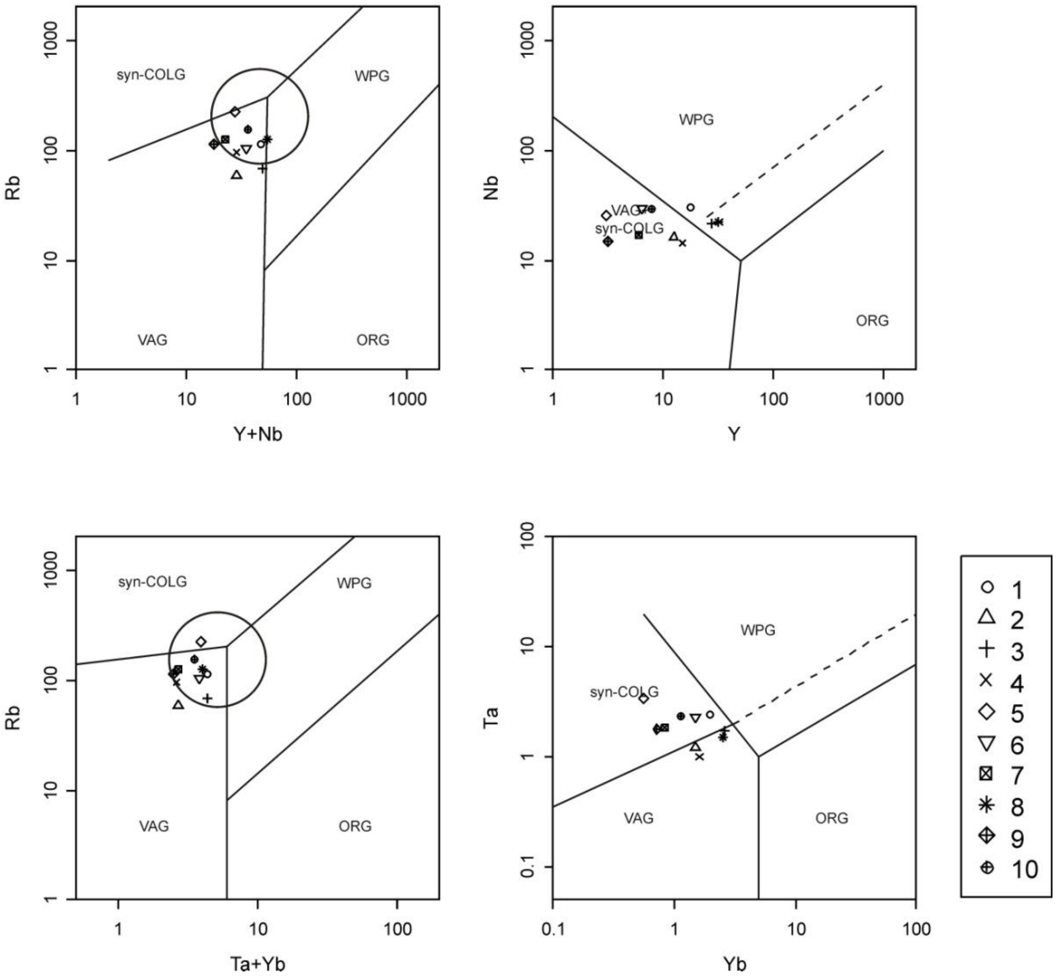

Figure. 7.7: Tectonic discrimination plots by Pearce et al., (1984), these plots suggests syn-collision to post-collision environment of granitic emplacement (WPG = Within Plate Granite, ORG = Oceanic Ridge Granite, VAG = Volcanic Arc Granite, Syn-COLG = Syn-collision Granites, Post-collision = Post-collision Granites).

The spider plots prepared by plotting of trace elements against various normalized values can serve as a tool for discriminating the granites on the basis of distinct pattern. The oceanic ridge granite (ORG) normalized geochemical pattern can be utilized to discriminate between major tectonic settings of granitic emplacement. In the (Fig. 7.8a) the ideal spider plot containing values for definite granitic suites of syn-collision type (Tibet, Yunnan, SW England and Barousse) is shown (Pearce et al., 1984). These patterns can be used in present study to compare the results acquired through trace element data for Godhra granites (Fig. 7.8b). Comparison of these patterns depicts syn-collision nature of granites. Chondrite normalized pattern of trace elements, the high normalized Ta values relative to the adjacent negative Nb anomaly is a typical characteristic of syn-collision granites (Harris et al., 1986). Similar characteristics are also observed in the granites of study area (Fig. 7.9) which further corroborate the syn-collision tectonic environment of granitic emplacement.

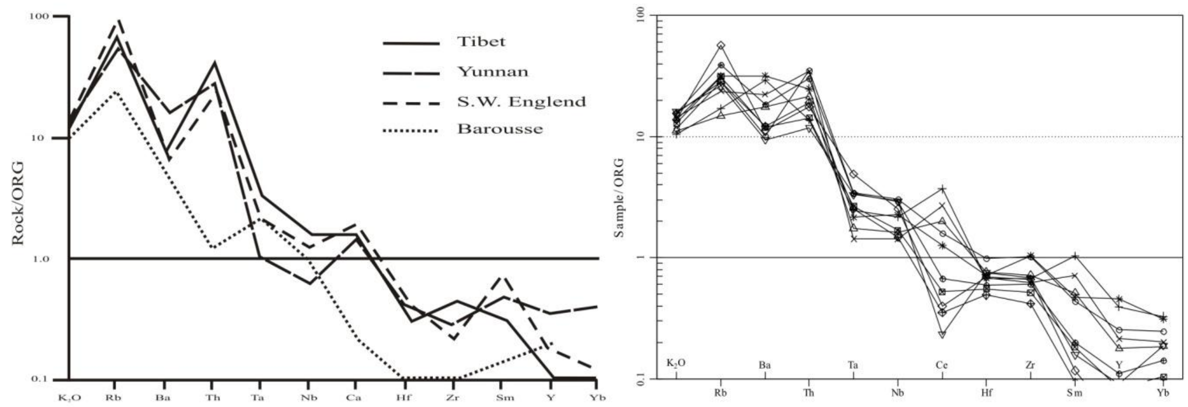

Figure. 7.8: (a) ORG normalized spider plot for ideal syn-collision granites (after, Pearce et al., 1984); (b) ORG normalized spider plot for 10 samples of granites of Study area.

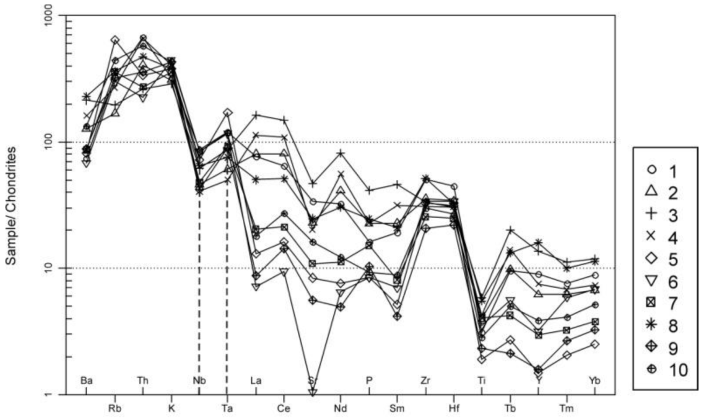

Figure. 7.9: Chondrite normalised pattern for granites of study area showing Ta enrichment with adjacent Nb anomaly. Thompson, (1982) data set used for normalization purpose.

7.6 Estimated temperature of the magma

Zircon saturation temperatures (T_{Zr}) calculated from bulk rock compositions provide a simple and robust means of estimating magma temperatures (Watson and Harrison, 1983; Miller et al., 2003). Watson and Harrison, (1983) have established experimentally that the partition coefficient of zircon $D^{Zr(Zircon/melt)}$ is a function of the parameter M [(Na + K + 2Ca)/(Al $*$ Si), all in cation fraction] and temperature. Therefore, using this formula, the Zr thermometry yields the temperature at which the granites of study area formed. The temperature derived for each sample is given in the following table (Table. 7.3).

Table. 7.3: Zircon Saturation Temperature

Sample No.	M	T_{Zr} (^{o}C)
TMG-1	1.58	842.3
TMG-2	1.38	825.7
TMG-3	1.76	789.7
TMG-4	1.48	803.9
TMG-5	1.34	821.2
TMG-6	1.22	832.8
TMG-7	1.34	798.4
TMG-8	1.50	851.3
TMG-9	1.29	783.3
TMG-10	1.25	819.5
Average Temperature =		816.8

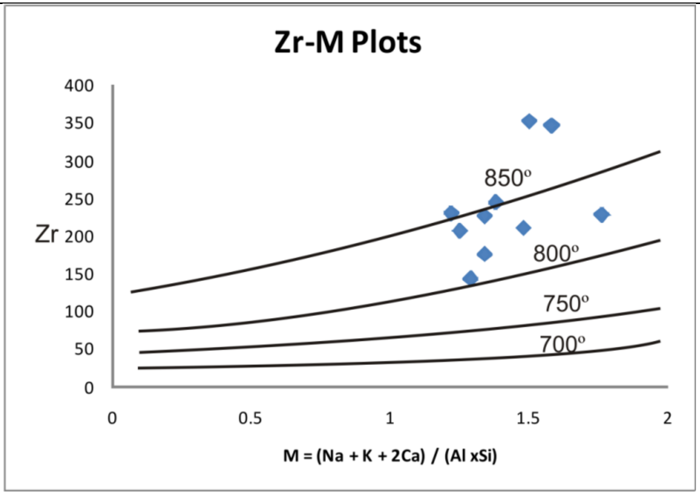

Figure. 7.10: Zr-M plots for estimation of zircon saturation temperature, after Watson and Harrison, (1983).

Based on the results, the estimated average temperature for granites of study area is 816.8˚C. This high temperature nature of granites may suggest that they have been generated at deeper level into the crust. The decreasing Zr content with increasing differentiation for all samples in accordance with their zircon saturation temperatures indicates that with progressive fractionation, the solubility of Zr decreases in the melt because of falling temperature and, consequently, zircon is being removed from the melt (King et al. 1997). Thus, The linear geochemical trends of major and trace elements illustrated by decreasing CaO, MgO, FeO(T), TiO_2, P_2O_5, Sr, Y and Zr and enrichment of LREE over HREE collectively suggest a major role of crystal fractionation in the petrogenesis of these granites (Fig. 7.10).

----------*END*----------